



Towards Large-Scale Daily Snow Density Mapping with Spatiotemporally Aware Model and Multi-Source Data

Huadong Wang¹, Xueliang Zhang¹, Pengfeng Xiao¹, Tao Che², Zhaojun Zheng³, Liyun Dai², Wenbo Luan¹

5 ¹Jiangsu Provincial Key Laboratory of Geographic Information Science and Technology, Key Laboratory for Land Satellite Remote Sensing Applications of Ministry of Natural Resources, School of Geography and Ocean Science, Nanjing University, Nanjing, Jiangsu 210023, China.

²Key Laboratory of Remote Sensing of Gansu Province, Heihe Remote Sensing Experimental Research Station, Cold and Arid Regions Environmental and Engineering Research Institute, Chinese Academy of Sciences, Lanzhou 730000, China.

10 ³The National Meteorological Satellite Meteorological Center, Beijing 100081, China.

Correspondence to: Xueliang Zhang (zxl@nju.edu.cn)

Abstract. Snow density plays a critical role in estimating water resources and predicting natural disasters such as floods, avalanches, and snowstorms. However, gridded products for snow density are lacking for understanding its spatiotemporal patterns. In this study, considering the multiple influencing variables and the strong spatiotemporal heterogeneity of snow density, the geographically and temporally weighted neural network (GTWNN) model is constructed for estimating daily snow density in China from 2013 to 2020, with the support of satellite, ground, and reanalysis data. The R^2 and RMSE achieve 0.515 and 0.043 g/cm³, respectively. The constructed GTWNN model is able to improve the estimation of snow density by capturing the weak and nonlinear relationship between snow density and the meteorological, snow, topographic, and vegetation variables. The leaf area index of high vegetation, snow depth, and topographic variables make a relatively great contribution for estimating snow density among the 17 influencing variables. The importance of addressing the spatiotemporal heterogeneity for snow density estimation is further demonstrated by comparing the GTWNN model with other models. The performance of the GTWNN model is closely related to the state and amount of snow, in which more stable and plentiful snow would result in higher snow density estimation accuracy. With the benefit of the daily snow density map, we obtain knowledge of the spatiotemporal pattern and heterogeneity of snow density in different snow periods and snow cover regions in China. The proposed GTWNN model holds the potential for large-scale daily snow density mapping, which will be beneficial for snow parameter estimation and water resource management.

1 Introduction

Seasonal snow cover occupies an important position in the global surface energy balance, hydrological cycle, and climate system (Bormann et al., 2018; Hall and Qu, 2006; Hernández et al., 2015; Li et al., 2018), which accounts for approximately 30 50% of the land area in winter in the Northern Hemisphere (Frei and Robinson, 1999). Snowmelt water not only provides fresh water for one-sixth of the world's population, but also affects agriculture and ecosystems downstream (Barnett et al., 2005).



Snow density is an important variable of snowpack, which influences the thermal, mechanical, and optical properties of snow layers (Surendar et al., 2015). It plays an important role in predicting natural disasters such as floods, avalanches, and snowstorms, establishing hydrological models, as well as water resources management (Fayad et al., 2017; Judson and
35 Doesken, 2000; Roebber et al., 2003; Schweizer et al., 2003).

Snow water equivalent (SWE) is critical for evaluating the contribution of snow cover to water resources (Niedzielski et al., 2019; Varade et al., 2020), which can be obtained by multiplying snow depth (SD) and snow density. Since the 1970s, algorithms for retrieving SD using passive microwave remote sensing have been continuously optimized (Chang et al., 1987; Gharaei-Manesh et al., 2016; Pulliainen et al., 1999). However, the SWE products obtained by passive microwave remote
40 sensing are mostly produced with a fixed value of snow density (Che et al., 2016; Pulliainen et al., 2020), due to the limited knowledge of snow density distribution. The snow density changes with time, and there is also strong spatial heterogeneity (Yang et al., 2019; Zhong et al., 2014). Snow density serves as a key variable for the accuracy of SWE products (McCreight and Small, 2014; Zaremehrijardy et al., 2021). For example, Yang et al. (2020) evaluated the accuracy of the GlobSnow-2 SWE product and found that using a fixed snow density to convert SD to SWE would cause the SWE to be overestimated in China.
45 Therefore, the production of daily gridded snow density products will benefit the estimation of SWE.

The fresh snow density is determined by the environment of falling snow, such as air temperature, relative humidity, and air pressure. After that, the size, shape, and packing of snow crystals are affected by the accumulation, sublimation, and melting of snow crystals on the surface, which leads to changes in snow density (Nakaya, 1951; Roebber et al., 2003). The snow density will also increase with snow age and SD due to the metamorphism and compaction, and the change rate is mainly
50 influenced by melt-refreeze events and wind erosion (Bormann et al., 2013; Meløysund et al., 2007). For example, the snow density in Northwest and Northeast China from 1999 to 2008 was found to be closely related to SD, as indicated by stepwise regression analysis of snow density and temperature, precipitation, SD, and wind speed (Dai and Che, 2011). In addition, the terrain and surface types also play an important role in snow density (Clark et al., 2011; Judson and Doesken, 2000). For example, snow density was found to be lower at higher elevations and on slopes that received less radiation (Wetlaufer et al.,
55 2016), and decreased by approximately 0.006 g/cm^3 with each 100 m increase in elevation. The average snow density in forest areas was 8%–13% less than that in open areas (Zhong et al., 2014).

The spatial and temporal differences in the distribution of multiple complex influencing variables result in obvious spatiotemporal heterogeneity of snow density. In the former Union of Soviet Socialist Republics (USSR), snow density will increase with latitude, while the snow density of the Altai Mountains in China is more related with longitude (Zhong et al.,
60 2014, 2021b). The average snow density shows obvious inter-monthly variation in the three major seasonal snow cover areas of China from 1957 to 2009 (Ma and Qin, 2012), and the monthly maximum snow density moved from north to south from October to January (Dai and Che, 2011). Moreover, this spatiotemporal heterogeneity is also reflected in the relationship between snow density and its influencing factors. The SD is often used to estimate snow density by different models (Lundberg et al., 2006; Sturm et al., 2010). However, the relationship between them is not robust in different time and space, where the



65 positive and negative relationship and the significance of correlation coefficient vary greatly at small scales (López-Moreno et al., 2013).

To understand the spatiotemporal heterogeneity of snow density, people often use the ground observation data, but it is difficult to achieve large-scale monitoring due to the complex environment and limited number of the stations. One method to explain the spatial and temporal variations in snow density is to use a physical model, such as the coupled energy and mass-
70 balance model ISNOBAL (Hedrick et al., 2018; Marks et al., 1999), which can explicitly simulate a number of snowpack properties including snow density and SWE. However, snow density physical models are complex and cannot achieve large-scale spatialization of snow density (Raleigh and Small, 2017). Another common method is to use statistical models trained by the climatic and snow variables to produce snow density map, such as multiple linear regression (MLR) and binary regression tree analysis (Meløysund et al., 2007; Mizukami and Perica, 2008; Wetlaufer et al., 2016). However, the simple
75 statistical models may not well capture the complicated nonlinear relationship of multiple influencing variables for snow density. More importantly, the models were mostly constructed for each observation independently and neglected the spatiotemporal heterogeneity of snow density as well as the relationship to its influencing variables.

Geographically weighted regression (GWR) is a model that considers spatial heterogeneity by using local multiple linear regression technology (Fotheringham et al., 1998). To further incorporate temporal dependency, geographically and temporally
80 weighted regression (GTWR) model has been introduced for many disciplines, such as meteorology, hydrology, and social economics (Chen et al., 2017; He and Huang, 2018; Huang et al., 2010). The machine learning approaches such as Random Forests (RF) (Breiman, 2001) and General Regression Neural Network (GRNN) (Specht, 1991) have become popular to fit nonlinear relationships, and it is in the initial stage for estimating snow density (Broxton et al., 2019). Consequently, we can incorporate geographical and temporal weight into a neural network model to establish a spatiotemporally varying nonlinear
85 relationship between snow density and its influencing variables, which not only considers the spatiotemporal heterogeneity for snow density, but also explains the nonlinear relationship between snow density and different influencing variables.

The main objectives of this study are (1) to develop a geographically and temporally weighted neural network (GTWNN) model for improving snow density mapping by addressing the spatiotemporal heterogeneity and capturing the nonlinear relationship between snow density and its influencing variables; (2) to validate the effectiveness of the proposed model in
90 various situations and to understand how the influencing variables affect snow density estimation; and (3) to achieve daily snow density mapping by integrating satellite, ground, and reanalysis data and to understand the spatiotemporal pattern of snow density in China.

2 Study Area and Data

2.1 In Situ Snow Density

95 We aim to achieve snow density mapping in China (Figure 1), where Xinjiang, Northeast China-Inner Mongolia, and the Tibetan Plateau are the three major regions with stable seasonal snow cover, covering a total area of approximately 4,200,000



several decades at a spatial resolution of $0.1^\circ \times 0.1^\circ$ (<https://cds.climate.copernicus.eu>) (Muñoz-Sabater, 2019). We extract the 10 m u-component of wind (U10), 10 m v-component of wind (V10), 2 m temperature (T2M), surface pressure (SP), total precipitation (TP), snowmelt (SMLT), snowfall (SF), temperature of snow layer (TSN), snow evaporation (ES), and leaf area index of high vegetation (LAI_HV), and calculate their daily average or accumulation accordingly.

115 The satellite products of snow albedo (SA), snow depth (SD), and snow cover area (SCA) from 2013 to 2020 are collected from the National Cryosphere Desert Data Center (<http://www.ncdc.ac.cn>) (Hao et al., 2021b; Xiao et al., 2020; Yang et al., 2019), with spatial resolutions of 0.01° , 25 km, and 5 km, respectively. Based on the SCA data, the snow cover duration (SCD) is calculated to account for the impact of gravity on snow density.

120 The topographical variables of elevation, slope, and aspect are obtained from the Shuttle Radar Topography Mission (SRTM) digital elevation model with a spatial resolution of 30 m.

2.3 Data Integration

First, the min-max normalization method is applied to normalize different influencing variables. In addition, since the spatial resolution varies among the different satellite data and reanalysis data, they are resampled to 25 km for snow density mapping. The spatial resolution of 25 km is determined to match that of most SD and SWE products by passive microwave remote
125 sensing. Accordingly, the ground observations of snow density measured at multiple sites are averaged for each 25 km grid cell. In total, we collect 16935 samples for model establishment and validation, where a sample refers to a grid cell with ground observations of snow density and its influencing variables.

3 Methodology

3.1 GTWNN Model

130 The schematic of the GTWNN model is shown in Figure 2, which consists of a geographically and temporally weighted (GTW) model to capture spatiotemporal heterogeneity and a generalized regression neural network (GRNN) to deal with the weak and nonlinear relationships between snow density and its influencing variables, including the meteorological variables, snow variables, topographical variables, and vegetation variables. The GTW model explores the spatiotemporal heterogeneity through local weighting, which can assess the impact of sample points on prediction points in terms of the spatial and temporal
135 distances. The weight of each sample point is calculated by the commonly used bi-square function (Guo et al., 2008), as shown in Eq. (1) and (2).

$$W_{GT}^i = \begin{cases} \left[1 - \left(\frac{d_{ST}^i}{h_{ST}}\right)^2\right]^2, & d_{ST}^i < h_{ST} \\ 0, & d_{ST}^i \geq h_{ST} \end{cases}, \quad (1)$$

$$d_{ST}^i = \sqrt{\left[(j_p - j_s^i)^2 + (k_p - k_s^i)^2\right] + \varphi(t_p - t_s^i)^2}, \quad (2)$$



where W_{GT}^i indicates the weight of the i_{th} ($i=1, 2, \dots, N$) sample point in the GTW model and d_{ST}^i denotes the spatial and
 140 temporal distance between the sample point and the prediction point. The spatiotemporal nonnegative parameters known as
 bandwidth h_{ST} and scale factor φ are the two key parameters in the GTW model (Huang et al., 2010). In essence, there are
 two weighting regimes for setting h_{ST} : fixed kernel and adaptive kernel. To reduce the “weak data” problem, that is, the spatial
 distribution of snow density observations is uneven, the adaptive kernel is selected to adapt the localization patterns of the
 observations by changing the kernel size automatically. The kernel will be large in regions with sparsely distributed
 145 observations and small when the data are abundant. The scale factor φ balances the different effects of the spatial and temporal
 distances in their respective metric systems. When $\varphi=0$, the temporal distance has no effect on the weight, indicating that the
 sample at any time will be considered. When $\varphi=\infty$, only the samples with the same date of the prediction point have an
 influence on the prediction, and GTW degrades into the classic geographically weighted (GW) model.

A common GRNN architecture consists of four layers. The first layer is the input layer receiving the influencing
 150 parameters, the number of neurons is equal to the input vector dimension N , and the number of influencing variables is m . The
 pattern layer is the radial base layer, and the weight of each neuron i in the pattern layer W_{GRNN}^i is calculated by the difference
 in the influencing variables between the sample and prediction points using a Gaussian function:

$$W_{GRNN}^i = e^{-\frac{1}{2} \left(\frac{D(x_p - x_s^i)}{spread} \right)^2}, \quad (3)$$

where x_s^i and x_p represent the influencing variable values of the sample and prediction points; $D()$ refers to the Euclidean
 155 distance; and $spread$ is a parameter to control the smoothness of the fitting function. Successively, there are two kinds of
 neurons in the summation layer. One is the denominator unit (S_W) for calculating the algebraic sum of each neuron, in which
 the weight of each neuron i in the summation layer is the snow density of sample point y_i , and the other is the molecular
 unit (S_S) for calculating the weighted sum of the pattern layer neurons. Finally, by combining the GTW and GRNN, the output
 snow density of the prediction point can be expressed as Eq. (4), where W_{GT}^i captures the spatiotemporal heterogeneity and
 160 W_{GRNN}^i relates to the nonlinear relationship between snow density and its influencing variables.

$$snow\ density = \frac{S_W}{S_S} = \frac{\sum_i^N (W_{GT}^i \cdot W_{GRNN}^i \cdot y_i)}{\sum_i^N (W_{GT}^i \cdot W_{GRNN}^i \cdot 1)}, \quad (4)$$

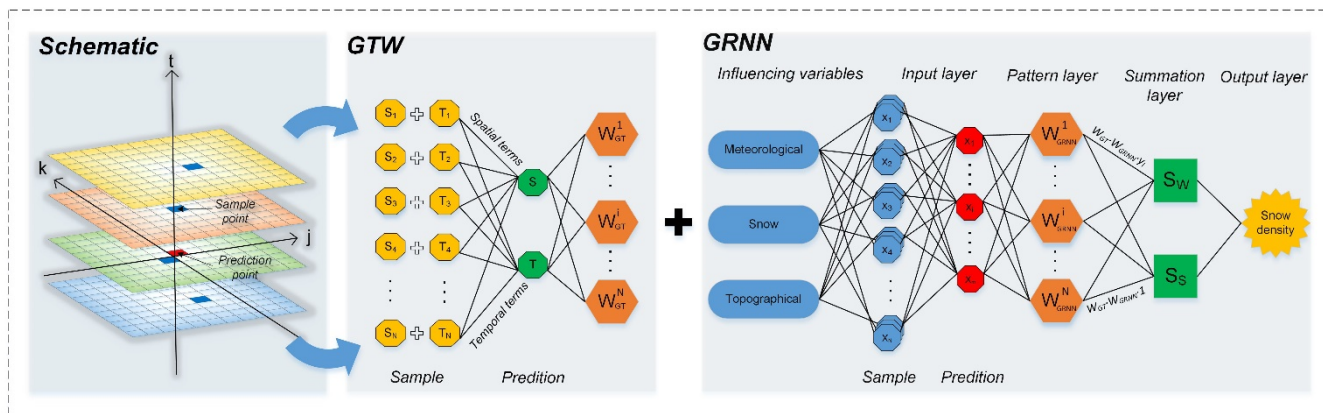


Figure 2. Schematic of the GTWNN model for the estimation of snow density.

3.2 Model Evaluation

165 There are three essential parameters in the GTWNN model, including the spatiotemporal bandwidth h_{ST} and the scale factor φ of the GTW model and the *spread* of GRNN model. The 10-fold cross-validation technique is adopted for determining the optimal parameters (Fotheringham et al., 2003; Rodriguez et al., 2010); that is, all the collected samples are randomly divided into 10 folds, nine folds are exploited for the model fitting, and one fold is used for the validation. Finally, a scale factor φ of 0.01, *spread* of 0.5, and an adaptive bandwidth regime h_{ST} of 8 with the best model performance are obtained.

170 4 Results

4.1 Descriptive Statistics of Ground Observations

175 Snow density has strong spatiotemporal heterogeneity, and we calculated statistics of the ground observations of the 16935 generated samples in terms of the snow density and the number of observations in different years, months, and snow cover regions, as shown in Figure 3. The snow density averaged in China from 2013 to 2020 is 0.14 g/cm^3 . The mean and median snow density values change slightly from 2013 to 2020 except for the fluctuation in 2019 with a snow density of 0.180 g/cm^3 . For the monthly variation, the mean snow density tends to increase from 0.120 g/cm^3 in October with the accumulation of snow and achieves the highest value of 0.162 g/cm^3 in March. Snow density also varies spatially. Among the three major snow cover regions, Xinjiang has the largest mean snow density (0.159 g/cm^3), followed by the Tibetan Plateau and Northeast China-Inner Mongolia.

180 In addition to the spatiotemporal variation in snow density, the number of ground observations also varies. The number of observation samples from 2013 to 2018 ranged from 2250 to 3250 but decreased to less than 750 in 2019 and 2020, mainly because of the lack of observations at many meteorological stations. The number of observation samples varies in different months mainly because of the richness of snow, which is higher in the snow stable period than in other periods. The number



185 of observation samples varies spatially mainly because of the distribution of meteorological stations, where the Northeast China-Inner Mongolia has the most stations, followed by Xinjiang and Tibetan Plateau.

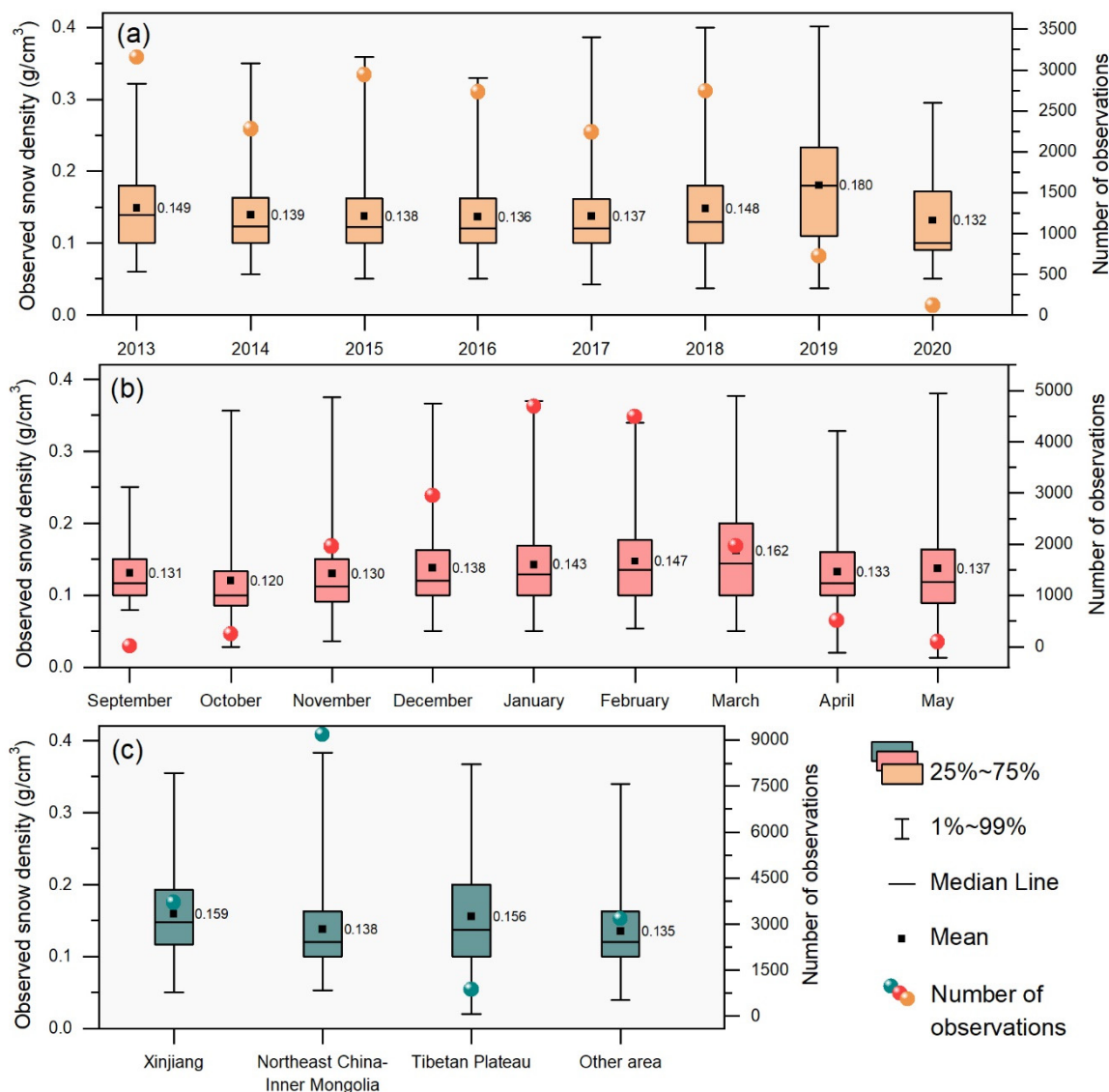


Figure 3. Descriptive statistics of the snow density and the number of ground observations in different (a) years, (b) months, and (c) snow cover regions.



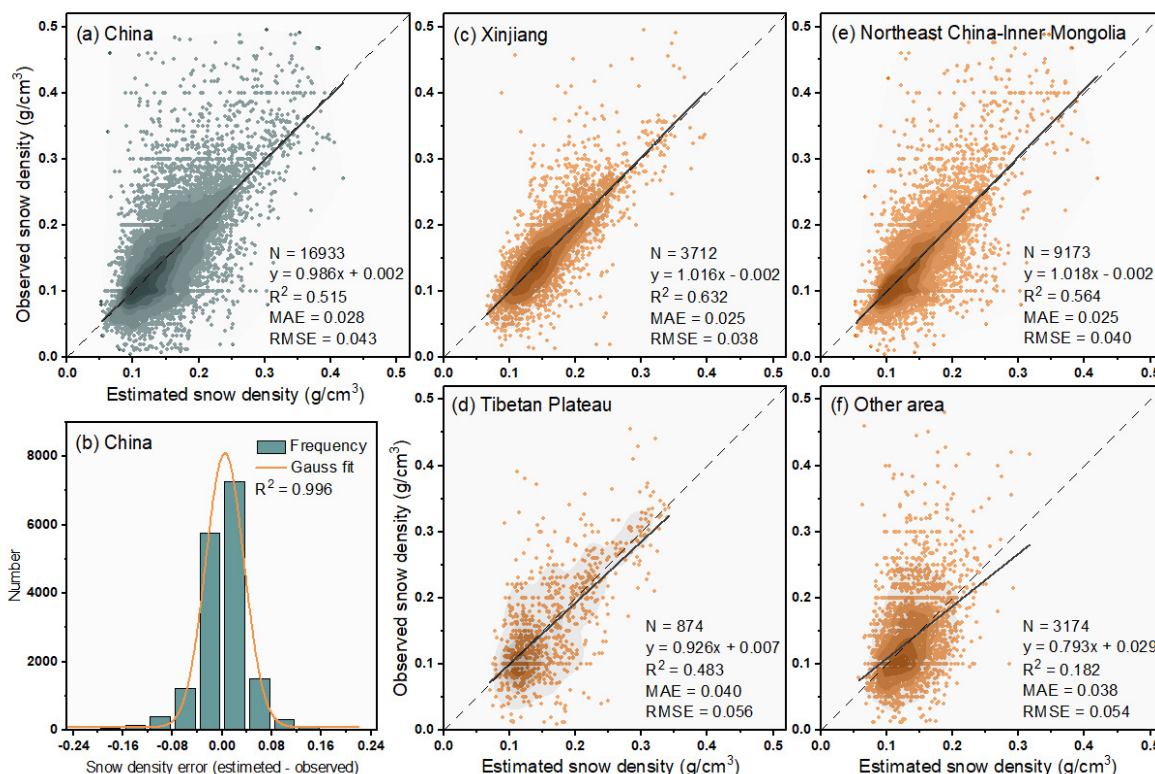
4.2 Model Validation

190 4.2.1 Accuracy of GTWNN Model in Different Regions

The snow density estimation accuracies of the GTWNN model are assessed for China (Figure 4a) and different snow cover regions, including Xinjiang (Figure 4c), Northeast China-Inner Mongolia (Figure 4e), Tibetan Plateau (Figure 4d), and other areas (Figure 4f). To clearly present the snow density errors between estimated values and observed values, the frequency of errors together with the Gaussian fitting curve are calculated and shown in Figure 4b.

195 Figure 4a shows that the R^2 , MAE, and RMSE values of China are 0.515, 0.028 g/cm³, and 0.043 g/cm³, respectively, which indicates that the GTWNN model is able to account for 51.5% of daily snow density variations. The linear fitting curve is very close to the 1:1 line with a slope of 0.986, and most of the points are concentrated on the trend line, especially in the range of 0.1–0.25 g/cm³. Figure 4b further demonstrates the concentration since most of the errors are smaller than ± 0.04 g/cm³. It is noted that the number of estimated values greater than 0.3 g/cm³ is rare, indicating that the GTWNN model would
200 underestimate the very large snow density.

Among the three stable seasonal snow cover regions, Xinjiang achieves the highest R^2 of 0.632 and the lowest RMSE of 0.038 g/cm³ and MAE of 0.025 g/cm³, followed by Northeast China-Inner Mongolia. Although Northeast China-Inner Mongolia has more observation samples than Xinjiang, the lower accuracies in Northeast China-Inner Mongolia would mainly be caused by the more forest cover and less stable snow cover in Northeast China-Inner Mongolia than in Xinjiang. The Tibetan
205 Plateau has the lowest R^2 of 0.483 and the highest RMSE and MAE, which is mainly caused by the high variety of snow density and sparse meteorological stations, as indicated in Figure 3c. Compared with the stable regions, the estimation accuracies in the other areas of China are apparently lower, with an R^2 of 0.182, which is caused by the rapid melting of snow and sparse observations.



210 **Figure 4. Accuracies of the estimated snow density in China (a) and different snow cover regions (c, d, e, and f) and the frequency distribution histogram of the snow density errors between estimated and observed values (b).**

4.2.2 Accuracy of GTWNN Model in Different Months

The snow density estimation accuracies of each month are assessed for the entire study area to reveal the effectiveness of the GTWNN model in different months, as shown in Table 1. In the snow season, the snow stable period achieves the best estimation performance with R^2 0.555, RMSE 0.040 g/cm³, and MAE 0.025 g/cm³. Within the snow stable period, the highest R^2 (0.566) appears in January, together with the lowest RMSE (0.038 g/cm³) and MAE (0.024 g/cm³), which is because of the stable snow state and the relatively sufficient observation samples.

The accuracies in the snow accumulation and snowmelt period are inferior to those in snow stable period, which is mainly caused by the relatively rapid changes in snow as well as the sparser observations, especially for the months of October, April, and May. It is noted that the accuracies in November and March are apparently higher than those in October, April, and May, mainly because the snow in these two months does not change so fast. The accuracies in September are not involved in the analysis because there are only 11 observations.



225 According to above results, we can safely conclude that the snow density estimation achieves the best performance in the snow stable period for the entire study area, and the estimations in November and March are also acceptable considering both the accuracies and the number of observations.

Table 1. Accuracies of snow density estimation in different months.

Snow cover period	Month	Number	Slope	R ²	RMSE	MAE
Snow accumulation period	September	11	1.443	0.545	0.035	0.030
	October	253	0.631	0.091	0.058	0.040
	November	1960	0.962	0.487	0.047	0.032
Snow stable period	December	2952	1.002	0.551	0.041	0.027
	January	4691	1.022	0.566	0.038	0.024
	February	4492	0.987	0.547	0.039	0.025
Snowmelt period	March	1972	0.973	0.482	0.053	0.036
	April	510	0.336	0.028	0.063	0.046
	May	92	0.729	0.107	0.069	0.050

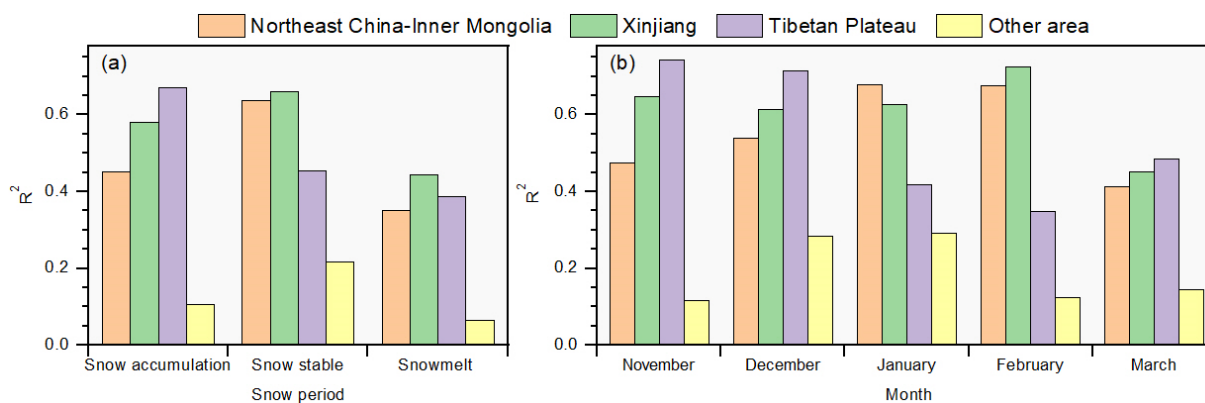
Furthermore, to clearly reveal the monthly accuracies of the GTWNN model in different snow cover regions, the snow density estimation accuracies for each snow period and part of the months are assessed in different snow cover regions, as shown in Figure 5.

230 In different snow periods, the snow stable period also achieves the highest R² in different snow cover regions except for the Tibetan Plateau, as shown in Figure 5a. The snow in Xinjiang, Northeast China-Inner Mongolia, and other areas of China is concentrated in the coldest months, and the state of snow is more stable in these months, resulting in a higher R². The accuracies on the Tibetan Plateau decrease from the snow accumulation period to the snowmelt period. This is because snow accumulates early and disappears late in the Tibetan Plateau, and the shallow snow depths make it difficult to maintain snow cover, resulting in more snow in autumn and spring and less snow in winter (Li and Mi, 1983; Zhong et al., 2021a). In addition, the snow changes rapidly in the snowmelt period, which results in a lower estimation accuracy in spring. Hence, combining the relatively large amount and the stable state of snow in the snow accumulation period, the snow density estimation accuracy is the highest in this period on the Tibetan Plateau.

240 We choose the three months of the snow stable period and November and March to analyse monthly accuracies in different regions because of the relatively higher overall accuracies in these months, as shown in Table 1, and the results are shown in Figure 5b. In most cases, the accuracies in Xinjiang, Northeast China-Inner Mongolia, and other areas of China first increase and then decrease from November to March and achieve the highest accuracies in January or February, when the snow cover is plentiful and stable. However, the accuracy on the Tibetan Plateau changes oppositely and achieves the highest accuracy in November because of the specialty of the snow amount changes within a year, as discussed above.



245 Therefore, we conclude that the accuracies of the GTWNN model are generally related to the stability and the amount of snow. The snow density estimations achieve the highest R^2 in the snow stable period in Xinjiang, Northeast China-Inner Mongolia, and other areas of China because of the concentration and stability of snow in this period, and achieve the highest R^2 during the snow accumulation period in the Tibetan Plateau because of the relatively large amount and stability of snow in this period.



250

Figure 5. Accuracies of snow density estimation in different snow periods (a) and months (b) of different snow cover regions.

4.2.3 Importance of the Influencing Variables for Snow Density Estimation

The GTWNN model is constructed separately for each year with the consideration of the snow variety in different years. The stepwise regression analysis method is used to filter the 17 influencing variables by performing the F test ($\alpha < 0.05$) and T test
 255 ($\alpha < 0.1$) to select significant variables for the GTWNN model in each year and calculate the Pearson correlation coefficient between snow density and the selected influencing variables to indicate the importance of the variables, as shown in Figure 6a. The selected variables and the corresponding correlation coefficient values are different among these years because of the snow variety. In addition, we calculate the average of the absolute value of the correlation coefficient and the number of selections in different years for each variable to clearly indicate the importance of the variables, as shown in Figure 6b. In
 260 general, the correlations between snow density and all influencing variables are not strong, with a maximum average correlation coefficient of only 0.202, which indicates the great difficulty for the estimation task of snow density.

For the 8 snow variables, SD shows apparently higher importance because it has the larger average correlation coefficient of 0.189 and is selected for modeling in each year. Among the 5 meteorological variables, the U10 has the highest average correlation coefficient of 0.165. It is noted that the number of selections for meteorological variables is apparently smaller than
 265 that for other variables. All three topographical variables show high importance, with average correlation coefficient values exceeding 0.1. Surprisingly, the variable LAI_HV has the largest average correlation coefficient among all the variables and is selected in most of the years, indicating the importance of vegetation for snow density estimation.



On the one hand, LAI_HV has the strongest correlation with snow density, followed by the SD, U10, and topographic variables among the 17 variables. On the other hand, the number of selected SD, LAI_HV, and topographic variables is apparently larger than that of U10. Accordingly, we assume that the variables LAI_HV, SD, and topographic variables are more relevant to the GTWNN model for snow density estimation than other variables.

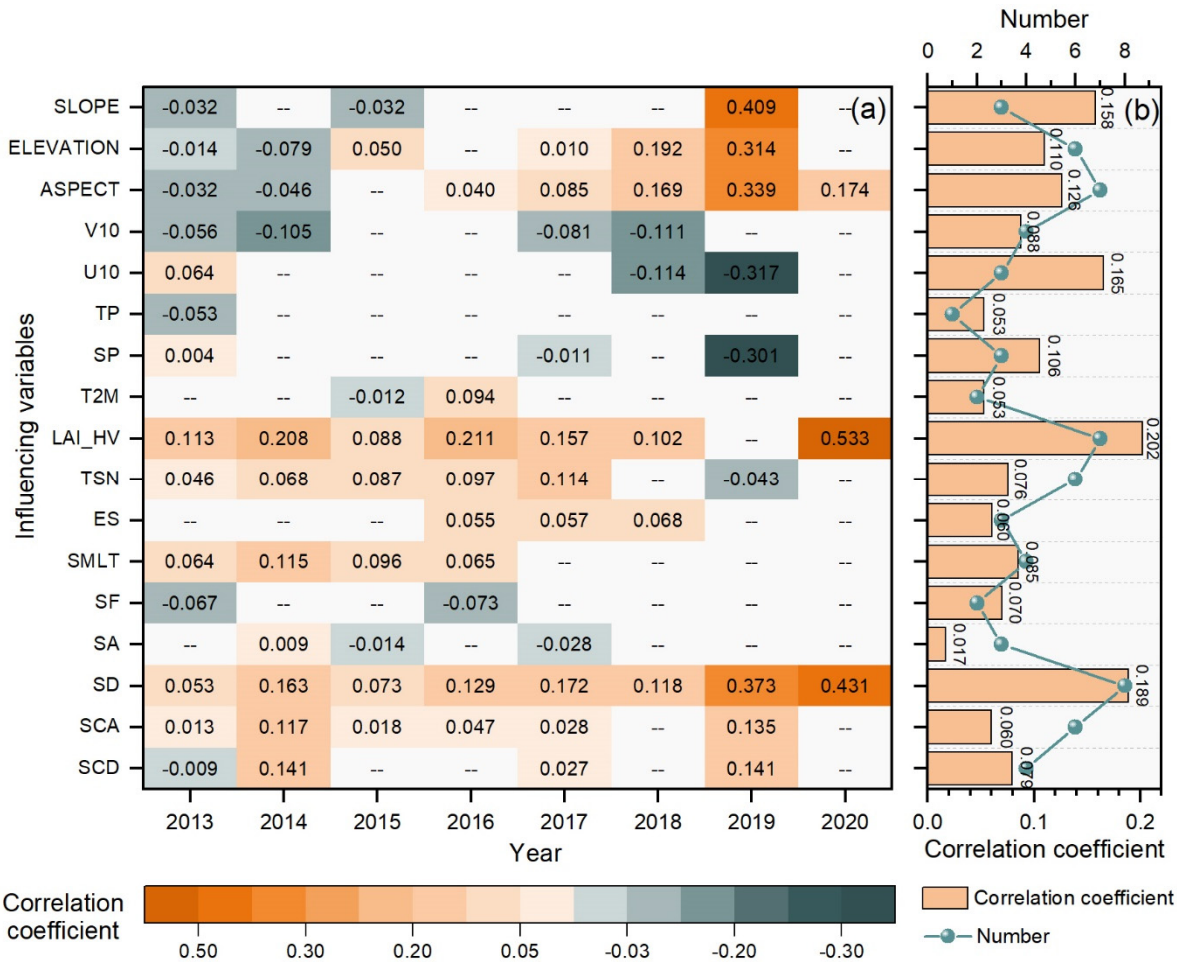


Figure 6. Correlation coefficient between snow density and its influencing variables selected by the stepwise regression method in each year (a), and the average of the absolute value of the correlation coefficient and the number of selections within these years (b).

275 4.3 Model Comparison

4.3.1 Comparison with Other Regression Models

The GTWNN model is compared with five other regression models to demonstrate its advantages for snow density estimation by considering the spatiotemporal heterogeneity of snow density and overcoming its weak correlation to influencing variables, as shown in Table 2. The models involved for comparison include the multiple linear regression (R), geographically weighted



280 regression (GWR), geographically and temporally weighted regression (GTWR), general regression neural network (GRNN),
and geographically weighted neural network (GWNN). It is noted that the GWNN model is constructed from the GTWNN
model by setting the scale factor $\varphi=\infty$, in which only the spatial weight is considered. The optimal parameters of the compared
models are determined by the 10-fold cross validation strategy as that for the GTWNN model.

285 The accuracies achieved by GTWNN are apparently higher than those achieved by GRNN and GWNN, which
demonstrates the effectiveness of both the spatial and temporal dependences on improving the estimation of heterogeneous
snow density. It is noted that the GWNN performs inferiorly to the GRNN model with only spatial dependence, which may be
caused by the sparse distribution of the stations and indirectly suggests that the temporal dependency makes a notable
contribution to improving the GRNN model. The similar accuracy differences among R, GWR, and GTWR also demonstrate
the importance of the spatial and temporal dependences for snow density estimation.

290 Comparing the GTWNN, GWNN, and GRNN models with the GTWR, GWR, and R models, the former three models
based on GRNN achieve apparently higher accuracies than the latter three models based on R. The accuracy differences mainly
come from the difference between the base regression models GRNN and R, where R is a linear model and GRNN can model
nonlinear relationships. Considering that the correlation coefficients between snow density and its influencing variables are
relatively weak, the results show that the nonlinear GRNN models can better overcome the weak correlations than the linear
295 R models.

Table 2. Accuracies of various models for estimating daily snow density.

Model	Slope	R ²	RMSE	MAE
R	1.089	0.069	0.060	0.044
GWR	0.176	0.047	0.087	0.057
GTWR	0.402	0.264	0.071	0.044
GRNN	1.261	0.166	0.057	0.041
GWNN	0.630	0.146	0.059	0.041
GTWNN	0.986	0.515	0.043	0.028

4.3.2 Comparison with Reanalysis Snow Density Product

300 The reanalysis product ERA-5 also provides the daily snow density grid data, which is produced by comprehensively
considering various influencing variables, such as snow pressure, viscosity, near surface air temperature, and wind speed
(Muñoz-Sabater, 2019). We compare the snow density estimated by the GTWNN model and that in ERA-5, and the results
are shown in Figure 7.

In Figure 7a, the R², RMSE, and MAE of ERA-5 snow density in the study area are 0.095, 0.061 g/cm³, and 0.047 g/cm³,
respectively, the performance of which is apparently inferior to that by the GTWNN model. The ERA-5 snow density is mostly
concentrated near 0.15 g/cm³, which leads to many overestimations and underestimations. Figure 7b and c further show that



305 the snow density estimated by the GTWNN model has higher accuracies than the ERA-5 product in different snow periods and different snow cover regions.

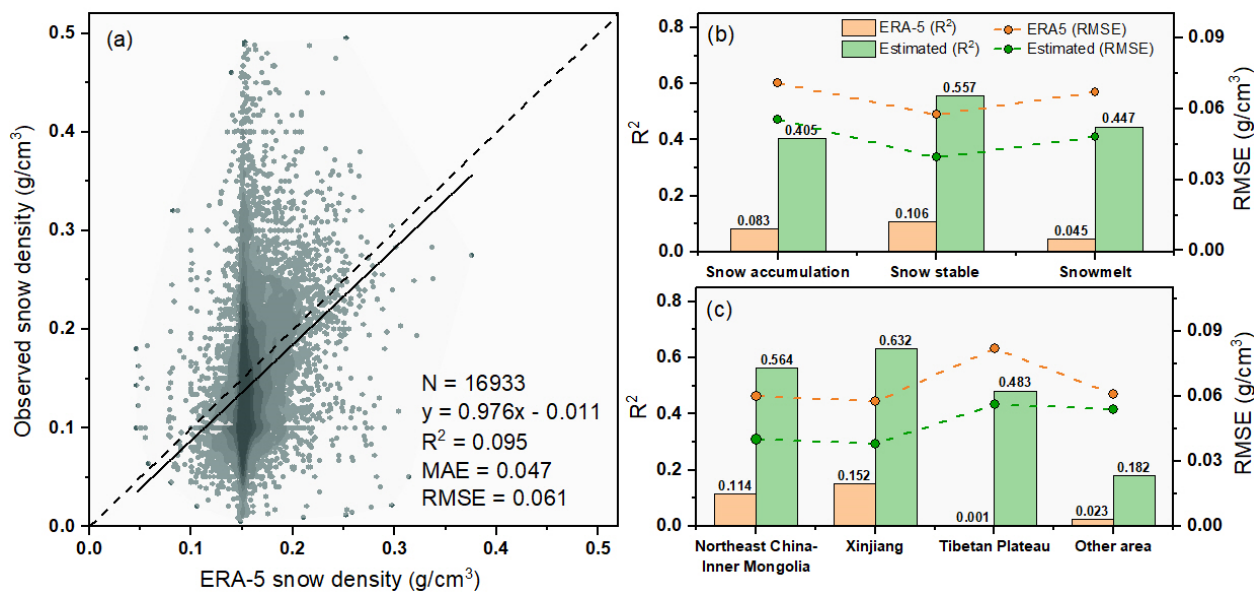


Figure 7. Accuracies of the ERA-5 snow density product in the entire study area (a) and the comparison of snow density estimated by the GTWNN model with that of ERA-5 in different snow periods (b) and different snow cover regions (c).

310 4.4 Mapping of Snow Density

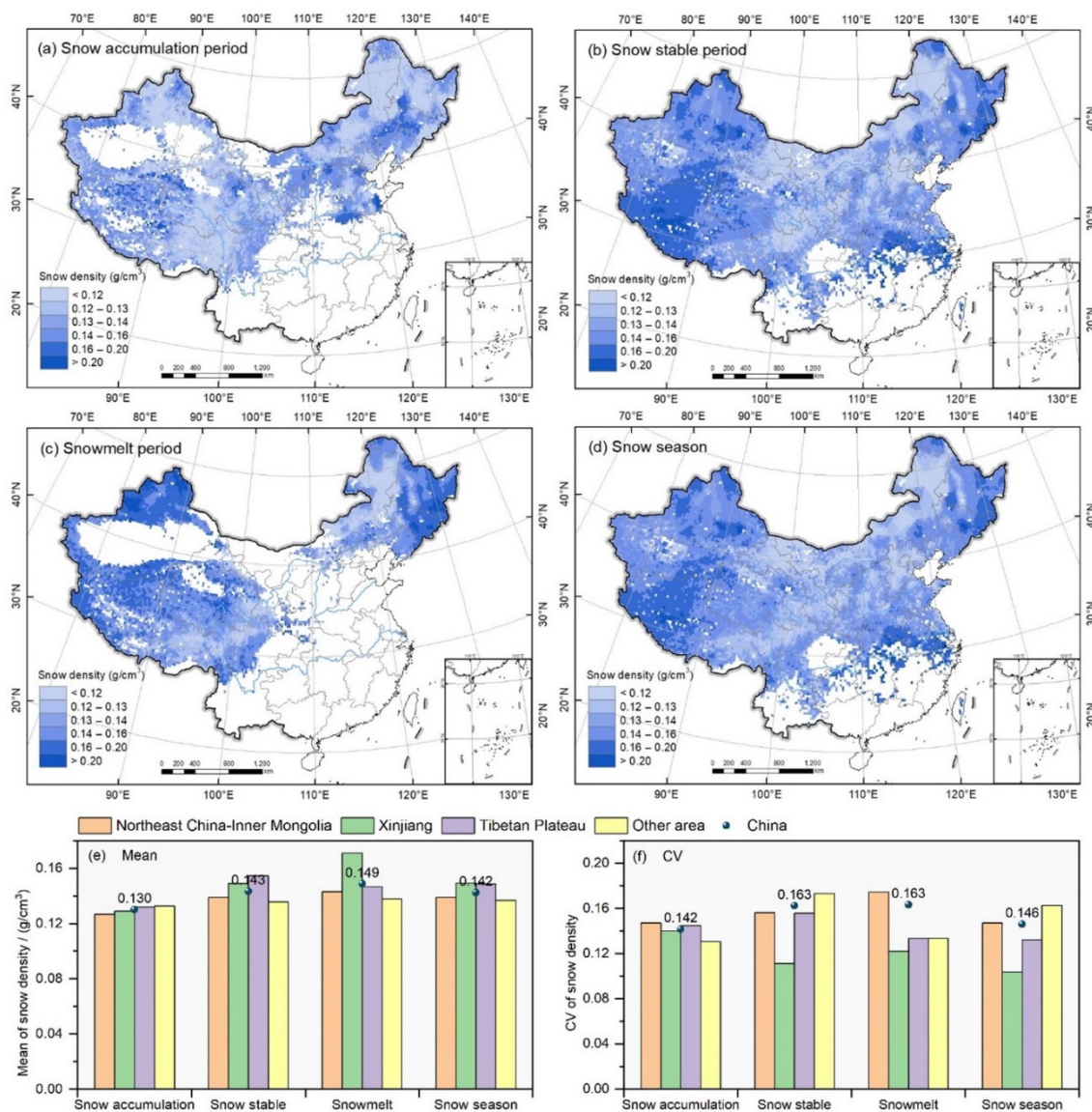
4.4.1 Spatial Distribution

The spatial distribution of snow density in different snow periods and the entire snow season in China are mapped and shown in Figure 8a–d by calculating the average of the daily snow density estimated by the GTWNN model from 2013 to 2020. It is noted that the estimated daily snow density maps are masked by the daily snow cover product to remove the nonsnow pixels (Hao et al., 2021b). In addition, to understand the spatiotemporal heterogeneity of snow density, we also calculate the mean snow density and coefficient of variability (CV) in different snow periods and regions, as shown in Figure 8e and f.

In the snow accumulation period, the mean snow density is generally lower than 0.13 g/cm³, except for the Northern Tibetan Plateau, Northeast Plain, and North China Plain. In the snow stable period, the mean snow density of China increases to 0.143 g/cm³, especially in Xinjiang and Tibetan Plateaus. In the snowmelt period, the mean snow density continues to increase to 0.149 g/cm³, especially increasing to 0.171 g/cm³ in northern Xinjiang and over 0.16 g/cm³ in Changbai Mountain of Northeast China. For the mean snow density of the entire snow season shown in Figure 8d, northern Xinjiang, the northwest Tibetan Plateau, and Northeast China have relatively higher snow density than Inner Mongolia and the southeast Tibetan Plateau in the three major snow cover regions. There is also a short snow period in the middle and lower reaches of the Yangtze River with relatively high snow density. The mean CV of snow density generally across China increases from snow



325 accumulation period (0.142) to snowmelt period (0.163). However, the CV in different snow cover regions varies apparently. It continuously increases in the Northeast China-Inner Mongolia from snow accumulation period to snowmelt period. However, the CV of Xinjiang achieves the lowest in the snow stable period, but that of the Tibetan Plateau reaches the highest in the snow stable period. Totally in the whole snow season, Xinjiang shows the lowest CV and Northeast China-Inner Mongolia has the largest CV.



330

Figure 8. Spatial distribution of mean snow density in different snow periods in China from 2013 to 2020, including the snow accumulation period (a), snow stable period (b), snowmelt period (c), and entire snow season (d), as well as the mean snow density (e) and CV (f) in different snow periods and snow cover regions.

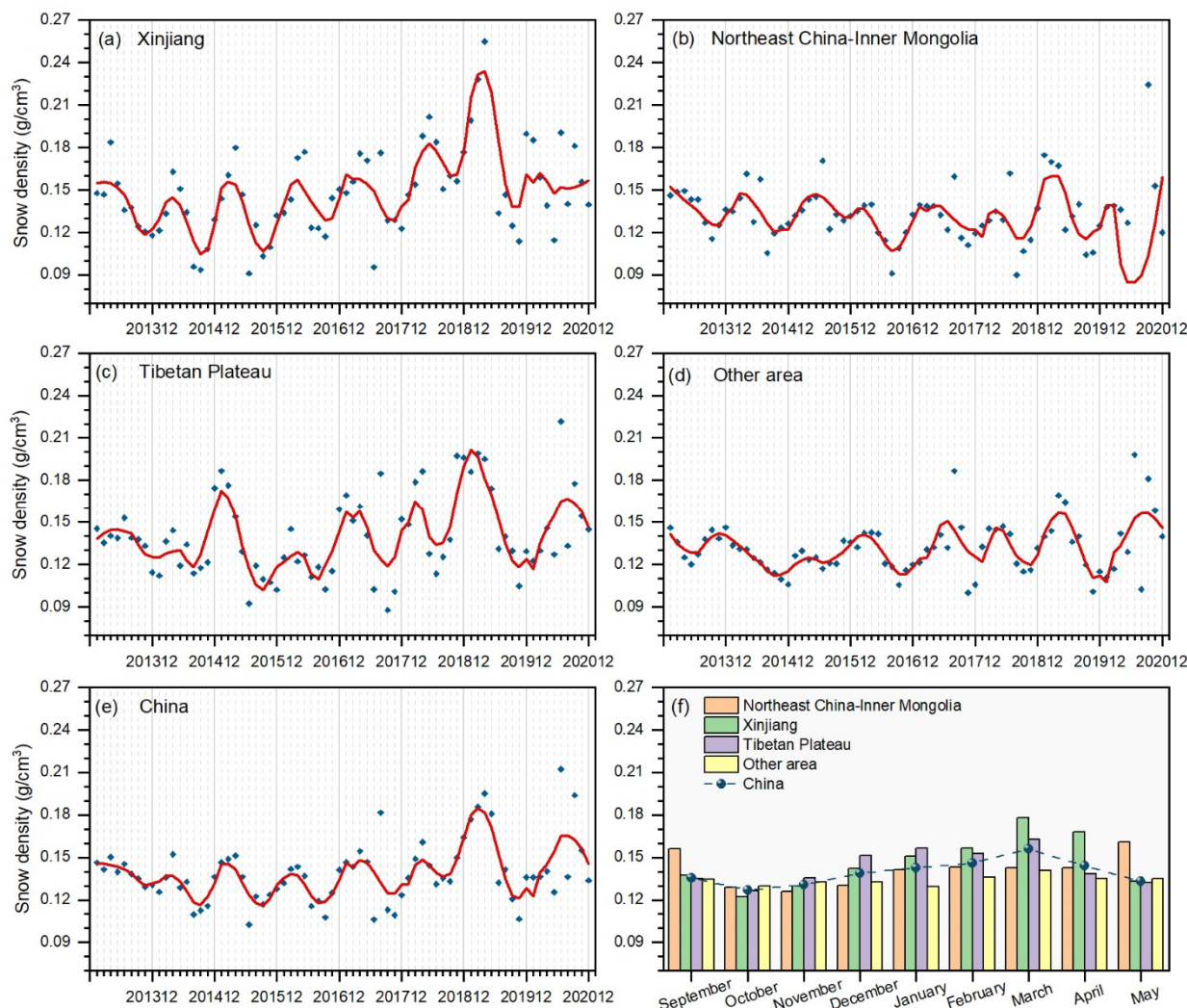


4.4.2 Temporal Change

335 To reflect the monthly change in snow density in different snow cover regions, we calculate the mean snow density in each month of the snow season from January 2013 to December 2020, as shown in Figure 9a–e, as well as the monthly mean snow density of the 8 years, as shown in Figure 9f.

Figure 9a–e shows that the snow density in different regions as well as the entire study area tends to increase from the start of snow accumulation to the peak and then decrease until the late snowmelt period in each year. However, the snow density fluctuations appear different over time. Specifically, the months with the maximum and minimum snow density are various in different years and regions. In addition, the maximum and minimum snow density values also fluctuate in different years and regions. The monthly mean snow density from the estimated daily snow density map in Figure 9f shows a similar pattern with that from the ground observations in Figure 3b, which further demonstrates the effectiveness of the proposed GTWNN model for snow density estimation. Figure 9b shows that the maximum snow density of the entire study area, Xinjiang, and Tibetan Plateau appears in March, as indicated by the monthly mean values. The monthly changes of Xinjiang and the Tibetan Plateau are similar and apparently different from those of Northeast China-Inner Mongolia.

340
345



350 **Figure 9.** Mean snow density in each month of the snow season from January 2013 to December 2020 in different snow cover regions, including Xinjiang (a), Northeast China-Inner Mongolia (b), Tibetan Plateau (c), other area (d), and the entire study area (e), and the monthly mean (f) snow density of the 8 years.

5 Discussion

5.1 Essential Issues of Constructing and Applying GTWNN Model

The constructed GTWNN model achieves daily snow density mapping by integrating a variety of influencing variables with the support of remote sensing, ground observation, and reanalysis data. Even though the validated accuracies are acceptable, 355 it is also necessary to address three essential issues for constructing and applying the model: (1) the weak correlation between



influencing variables and snow density, (2) the model evaluation and parameter estimation, and (3) the relation to the state of snow.

For the first issue, we found that the influencing variables have relatively limited explanatory abilities for estimating snow density, as indicated by the weak correlations in Figure 6, which may be an important reason for the low accuracy of the GTWNN model for snow density estimation with an R^2 of 0.515. For example, Li et al. (2020) established a GTWNN model for estimating ground-level $PM_{2.5}$ with the input of satellite-derived aerosol optical depth (AOD) and meteorological data, and the model achieved an R^2 value of 0.80, which may be related to the higher linear correlation between AOD and $PM_{2.5}$ with an R^2 of 0.75 (Xin et al., 2016). Considering the weak correlations between snow density and its influencing variables, it could be challenging to achieve very high estimation accuracy for snow density.

For the second issue, there are three essential parameters in the GTWNN model, including the scale factor φ and the spatiotemporal bandwidth h_{ST} , and the *spread*. Especially for the bandwidth, when we choose the adaptive bandwidth regime $h_{ST} = 6$, the R^2 of the estimated snow density could achieve a higher value of 0.541. However, there will be abnormal block patterns in the snow density map caused by the limited number of samples. Specifically, in a small area constrained by $h_{ST} = 6$, the same samples can be selected for estimating the snow density of different nearby grids. Since the spatiotemporal weights and the weights of influencing variables are too similar, it results in the block phenomenon with areas composed of grids with very similar snow density. Therefore, even though a relatively smaller h_{ST} could achieve a higher R^2 , we have to increase the bandwidth $h_{ST} = 8$ to avoid the abnormal block patterns that are inconsistent with our common sense.

For the third issue, it is noted that the accuracy of the snow density estimation model is closely related to the stability and amount of snow. The R^2 values in the three major snow cover regions are apparently higher than those in the other areas in China because of the more stable and larger amount of snow, as shown in Figure 4. In addition, the accuracy differences in different months show that the GTWNN model achieves higher performance when snow is more stable, such as the snow stable period, the late snow accumulation period, and the early snowmelt period. Hence, when applying the GTWNN model, if the snow is stable and plentiful, the estimated snow density would be more credible. In contrast, if the snow changes rapidly or distributes sparsely, such as in the early snow accumulation period and the late snowmelt period, the estimated snow density would be less credible and need to be used with caution.

5.2 Advantages and Limitations

Even though the ground measurement accuracy continues to improve by advanced measurement instruments (Hao et al., 2021a), it is limited to obtaining the large-scale spatial distribution of snow density, and gridded snow density data are urgently needed. To obtain the gridded snow density, snow parameters such as snow depth (Jonas et al., 2009; McCreight and Small, 2014) and meteorological data such as temperature and wind speed (Helfricht et al., 2018; Judson and Doesken, 2000; Valt et al., 2018) were used to estimate snow density mainly by using a linear regression model. The linear regression model is globally oriented and thus cannot effectively deal with the spatiotemporal heterogeneity of snow density. Accordingly, previous studies mostly achieve snow density estimation in regions that are not very large in size. The constructed GTWNN in this study



390 considers the spatial and temporal dependences of snow density, which allows it to effectively deal with the spatiotemporal
heterogeneity of snow density and thus hold the potential of being applied to large-scale areas, as demonstrated by the
apparently higher accuracies than the linear regression model in our study area. In addition, it is important to overcome the
weak correlation between snow density and its influencing variables to improve the estimation accuracy. Accordingly, we
make two efforts in the GTWNN model. First, 17 influencing variables are integrated for the estimation with the support of
multisource data, which allows us to apply the feature selection method to select the more relevant variables for estimation.
395 Second, the adopted GRNN model could overcome the nonlinear relationship between snow density and its influencing
variables.

It is noted that the confidence of the snow density map produced by the GTWNN model is still constrained by the
distribution of the observation stations, even though the model is able to achieve relatively high accuracy in regions with sparse
stations, e.g., the R^2 of 0.483 in the Tibetan Plateau. Since there are few observations, especially in the northwest Tibetan
400 Plateau, the confidence of the estimated snow density in this region is still not clear. On the one hand, we expect new
observations in the near future for both estimation and validation. On the other hand, it is of great potential to further develop
a snow density prediction model without the dependence of observed snow density for model inference.

6 Conclusion

A GTWNN model was constructed for snow density estimation and achieved daily snow density mapping from 2013 to 2020
405 in China with the support of remote sensing, ground observation, and reanalysis data. The GTWNN model has two advantages:
(1) considering the spatiotemporal heterogeneity of snow density, and (2) addressing the weak and nonlinear relationship as
well as the involvement of a variety of snow, meteorological, topographic, and vegetation variables. The GTWNN model
achieves an R^2 of 0.515, RMSE of 0.043 g/cm³, and MAE of 0.028 g/cm³ in China validated by 10-fold cross validation, which
are apparently better than those of the other five regression models and the ERA-5 snow density product. The comparison
410 results further demonstrate the importance of addressing the spatiotemporal heterogeneity for snow density estimation. The
performance of the GTWNN model is also demonstrated to be closely related to the state and amount of snow, in which more
stable and plentiful snow would result in higher snow density estimation accuracy. The importance of different influencing
variables is evaluated for estimating snow density and finding that the vegetation variable LAI_HV, snow variable SD, and
topographic variables make a relatively great contribution. With the benefit of the produced daily snow density map, we obtain
415 knowledge of the spatiotemporal pattern of snow density in different snow periods and snow cover regions in China, and the
CV results show that spatial heterogeneity of snow density in Northeast China-Inner Mongolia is the most obvious in three
major snow cover regions, and the least obvious in Xinjiang. The proposed GTWNN model has the potential to be used for
large-scale snow density mapping because of the two advantages described above but with limitations to the distribution of
the observation stations. Future work should focus on extending the model to other areas and longer time series as well as
420 developing snow density prediction models.



Data availability

Our research mainly uses three types of data, including the ground observation data, satellite remote sensing data, and reanalysis data. The daily snow depth and snow pressure measurements are collected from the China Meteorological Administration (CMA) and the National Cryosphere Desert Data Center (<http://www.ncdc.ac.cn>), we are not authorized to redistribute part of these data without permission. The remote sensing data we used are all open source data. The products of snow variables are available at the National Cryosphere Desert Data Center (<http://www.ncdc.ac.cn>), including the daily snow albedo, snow depth, and snow cover area from 2013 to 2020, and the Shuttle Radar Topography Mission (SRTM) digital elevation model (DEM) can be downloaded at <http://www.dsac.cn/DataP>. The reanalysis data are collected from the ECMWF ERA-5 land hourly dataset (<https://cds.climate.copernicus.eu>).

430 Author contribution

Xueliang Zhang and Pengfeng Xiao formulated the research goals; Huadong Wang, Zhaojun Zheng, Liyun Dai, and Tao Che performed the data curation; Huadong Wang and Xueliang Zhang analyzed the data and wrote the manuscript draft; Pengfeng Xiao, Tao Che, Zhaojun Zheng, Liyun Dai, and Wenbo Luan reviewed and edited the manuscript.

Competing interests

435 The authors declare that they have no conflict of interest.

Acknowledgments

This study is supported by the Special Subject of National Science and Technology Basic Resources Investigation (Grant No. 2017FY100503), the National Natural Science Foundation of China (Grant No. 42171307), the Fundamental Research Funds for the Central Universities (Grant No. 020914380095), and the High-level Innovation and Entrepreneurship Talents Introduction Program of Jiangsu Province of China.

References

Barnett, T. P., Adam, J. C., and Lettenmaier, D. P.: Potential impacts of a warming climate on water availability in snow-dominated regions, *Nature*, 438, 303–309, <https://doi.org/10.1038/nature04141>, 2005.
Bormann, K. J., Westra, S., Evans, J. P., and McCabe, M. F.: Spatial and temporal variability in seasonal snow density, *Journal of Hydrology*, 484, 63–73, <https://doi.org/10.1016/j.jhydrol.2013.01.032>, 2013.



- Bormann, K. J., Brown, R. D., Derksen, C., and Painter, T. H.: Estimating snow-cover trends from space, *Nature Clim Change*, 8, 924–928, <https://doi.org/10.1038/s41558-018-0318-3>, 2018.
- Breiman, L.: Random forests, *Mach. Learn.* 45, 5–32, <https://doi.org/10.1023/A:1010933404324>, 2001.
- Broxton, P. D., van Leeuwen, W. J. D., and Biederman, J. A.: Improving Snow Water Equivalent Maps with Machine Learning
450 of Snow Survey and Lidar Measurements, *Water Resources Research*, 55, 3739–3757, <https://doi.org/10.1029/2018WR024146>, 2019.
- Chang, A. T. C., Foster, J. L., and Hall, D. K.: Nimbus-7 SMMR Derived Global Snow Cover Parameters, *Annals of Glaciology*, 9, 39–44, <https://doi.org/10.3189/S0260305500200736>, 1987.
- Che T.: Snow survey dataset from measurement routes in the typical regions of China during 2017–2021, National Cryosphere
455 Desert Data Center (<http://www.ncdc.ac.cn>) [data set], <https://doi.org/10.12072/ncdc.I-SNOW.db0007.2021>, 2021.
- Che, T., Dai, L., Zheng, X., Li, X., and Zhao, K.: Estimation of snow depth from passive microwave brightness temperature data in forest regions of northeast China, *Remote Sensing of Environment*, 183, 334–349, <https://doi.org/10.1016/j.rse.2016.06.005>, 2016.
- Chen, B., Huang, B., Chen, L., and Xu, B.: Spatially and Temporally Weighted Regression: A Novel Method to Produce
460 Continuous Cloud-Free Landsat Imagery, *IEEE Transactions on Geoscience and Remote Sensing*, 55, 27–37, <https://doi.org/10.1109/TGRS.2016.2580576>, 2017.
- Clark, M. P., Hendrikx, J., Slater, A. G., Kavetski, D., Anderson, B., Cullen, N. J., Kerr, T., Hreinsson, E. Ö., and Woods, R. A.: Representing spatial variability of snow water equivalent in hydrologic and land-surface models: A review, *Water Resources Research*, 47, <https://doi.org/10.1029/2011WR010745>, 2011.
- 465 Dai, L. and Che, T.: Spatiotemporal distributions and influences on snow density in China from 1999 to 2008, *Sciences in Cold and Arid Regions*, 3, 325–331, <https://doi.org/10.3724/SP.J.1226.2011.00325>, 2011.
- Fayad, A., Gascoïn, S., Faour, G., López-Moreno, J. I., Drapeau, L., Page, M. L., and Escadafal, R.: Snow hydrology in Mediterranean mountain regions: A review, *Journal of Hydrology*, 551, 374–396, <https://doi.org/10.1016/j.jhydrol.2017.05.063>, 2017.
- 470 Fotheringham, A., Brunson, C., and Charlton, M.: Geographically Weighted Regression: The Analysis of Spatially Varying Relationships, *Geographical Analysis*, 35, 272–275, <https://doi.org/10.1111/j.1538-4632.2003.tb01114.x>, 2003.
- Fotheringham, A. S., Charlton, M. E., and Brunson, C.: Geographically weighted regression: a natural evolution of the expansion method for spatial data analysis, *Environment and Planning*, 30, 1905–1927, <https://doi.org/10.1068/a301905>, 1998.
- Frei, A. and Robinson, D. A.: Northern Hemisphere snow extent: regional variability 1972–1994, *Int. J. Climatol.*, 26,
475 [https://doi.org/10.1002/\(SICI\)1097-0088\(19991130\)19:14<1535::AID-JOC438>3.0.CO;2-J](https://doi.org/10.1002/(SICI)1097-0088(19991130)19:14<1535::AID-JOC438>3.0.CO;2-J), 1999.
- Gharaei-Manesh, S., Fathzadeh, A., and Taghizadeh-Mehrjardi, R.: Comparison of artificial neural network and decision tree models in estimating spatial distribution of snow depth in a semi-arid region of Iran, *Cold Regions Science and Technology*, 122, 26–35, <https://doi.org/10.1016/j.coldregions.2015.11.004>, 2016.



- Guo, L., Ma, Z., and Zhang, L.: Comparison of bandwidth selection in application of geographically weighted regression: a
480 case study, *Can. J. For. Res.*, 38, 2526–2534, <https://doi.org/10.1139/X08-091>, 2008.
- Hall, A. and Qu, X.: Using the current seasonal cycle to constrain snow albedo feedback in future climate change, *Geophysical
Research Letters*, 33, <https://doi.org/10.1029/2005GL025127>, 2006.
- Hao, J., Mind'je, R., Feng, T., and Li, L.: Performance of snow density measurement systems in snow stratigraphies,
Hydrology Research, 52, 834–846, <https://doi.org/10.2166/nh.2021.133>, 2021a.
- 485 Hao, X., Huang, G., Che, T., Ji, W., Sun, X., Zhao, Q., Zhao, H., Wang, J., Li, H., and Yang, Q.: The NIEER AVHRR snow
cover extent product over China – a long-term daily snow record for regional climate research, *Earth System Science Data*, 13,
4711–4726, <https://doi.org/10.5194/essd-13-4711-2021>, 2021b.
- He, Q. and Huang, B.: Satellite-based mapping of daily high-resolution ground PM_{2.5} in China via space-time regression
modeling, *Remote Sensing of Environment*, 206, 72–83, <https://doi.org/10.1016/j.rse.2017.12.018>, 2018.
- 490 Hedrick, A. R., Marks, D., Havens, S., Robertson, M., Johnson, M., Sandusky, M., Marshall, H.-P., Kormos, P. R., Bormann,
K. J., and Painter, T. H.: Direct Insertion of NASA Airborne Snow Observatory-Derived Snow Depth Time Series Into the
iSnoB Energy Balance Snow Model, *Water Resources Research*, 54, 8045–8063, <https://doi.org/10.1029/2018WR023190>,
2018.
- Helfricht, K., Hartl, L., Koch, R., Marty, C., and Olefs, M.: Obtaining sub-daily new snow density from automated
495 measurements in high mountain regions, *Hydrology and Earth System Sciences*, 22, 2655–2668, <https://doi.org/10.5194/hess-22-2655-2018>, 2018.
- Hernández-Henríquez, M. A., Déry, S. J., and Derksen, C.: Polar amplification and elevation-dependence in trends of Northern
Hemisphere snow cover extent, 1971–2014, *Environ. Res. Lett.*, 10, 044010, <https://doi.org/10.1088/1748-9326/10/4/044010>,
2015.
- 500 Huang, B., Wu, B., and Barry, M.: Geographically and temporally weighted regression for modeling spatio-temporal variation
in house prices, *Geographical Information Science*, 24, 383–401, <https://doi.org/10.1080/13658810802672469>, 2010.
- Huang, X., Deng, J., Ma, X., Wang, Y., Feng, Q., Hao, X., and Liang, T.: Spatiotemporal dynamics of snow cover based on
multi-source remote sensing data in China, *The Cryosphere*, 10, 2453–2463, <https://doi.org/10.5194/tc-10-2453-2016>, 2016.
- Jonas, T., Marty, C., and Magnusson, J.: Estimating the snow water equivalent from snow depth measurements in the Swiss
505 Alps, *Journal of Hydrology*, 378, 161–167, <https://doi.org/10.1016/j.jhydrol.2009.09.021>, 2009.
- Judson, A. and Doesken, N.: Density of Freshly Fallen Snow in the Central Rocky Mountains, *Bulletin of the American
Meteorological Society*, 81, 11, [https://doi.org/10.1175/1520-0477\(2000\)081<1577:DOFFSI>2.3.CO;2](https://doi.org/10.1175/1520-0477(2000)081<1577:DOFFSI>2.3.CO;2), 2000.
- Li P. and Mi D.: Distribution of snow cover in China, *Journal of Glaciology and Geocryology*, 04, 9-18, 1983. In Chinese.
- Li, T., Shen, H., Yuan, Q., and Zhang, L.: Geographically and temporally weighted neural networks for satellite-based mapping
510 of ground-level PM_{2.5}, *ISPRS Journal of Photogrammetry and Remote Sensing*, 167, 178–188,
<https://doi.org/10.1016/j.isprsjprs.2020.06.019>, 2020.



- Li, W., Guo, W., Qiu, B., Xue, Y., Hsu, P.-C., and Wei, J.: Influence of Tibetan Plateau snow cover on East Asian atmospheric circulation at medium-range time scales, *Nat Commun*, 9, 4243, <https://doi.org/10.1038/s41467-018-06762-5>, 2018.
- 515 López-Moreno, J. I., Fassnacht, S. R., Heath, J. T., Musselman, K. N., Revuelto, J., Latron, J., Morán-Tejeda, E., and Jonas, T.: Small scale spatial variability of snow density and depth over complex alpine terrain: Implications for estimating snow water equivalent, *Advances in Water Resources*, 55, 40–52, <https://doi.org/10.1016/j.advwatres.2012.08.010>, 2013.
- Lundberg, A., Richardson-Näslund, C., and Andersson, C.: Snow density variations: consequences for ground-penetrating radar, *Hydrological Processes*, 20, 1483–1495, <https://doi.org/10.1002/hyp.5944>, 2006.
- Ma, L. and Qin, D.: Spatial-Temporal Characteristics of Observed Key Parameters for Snow Cover in China during 1957—
520 2009, *Journal of Glaciology and Geocryology*, 34, 1–11, <https://doi.org/10.3724/SP.J.1226.2012.00384>, 2012.
- Marks, D., Domingo, J., Susong, D., Link, T., and Garen, D.: A spatially distributed energy balance snowmelt model for application in mountain basins, *Hydrological Processes*, 13, 1935–1959, [https://doi.org/10.1002/\(SICI\)1099-1085\(199909\)13:12/13<1935::AID-HYP868>3.0.CO;2-C](https://doi.org/10.1002/(SICI)1099-1085(199909)13:12/13<1935::AID-HYP868>3.0.CO;2-C), 1999.
- McCreight, J. L. and Small, E. E.: Modeling bulk density and snow water equivalent using daily snow depth observations, *The
525 Cryosphere*, 8, 521–536, <https://doi.org/10.5194/tc-8-521-2014>, 2014.
- Meløysund, V., Leira, B., Høiseith, K. V., and Lisø, K. R.: Predicting snow density using meteorological data, *Meteorological Applications*, 14, 413–423, <https://doi.org/10.1002/met.40>, 2007.
- Mizukami, N. and Perica, S.: Spatiotemporal Characteristics of Snowpack Density in the Mountainous Regions of the Western United States, *Journal of Hydrometeorology*, 9, 1416–1426. <https://doi.org/10.1175/2008JHM981.1>, 2008.
- 530 Muñoz-Sabater, J.: ERA5-Land hourly data from 1981 to present, Copernicus Climate Change Service (C3S) Climate Data Store (CDS). (Accessed on < 23-January-2021 >) [data set], <https://doi.org/10.24381/cds.e2161bac>, 2019.
- Nakaya, U.: The Formation of Ice Crystals, in: *Compendium of Meteorology: Prepared under the Direction of the Committee on the Compendium of Meteorology*, edited by: Byers, H. R., Landsberg, H. E., Wexler, H., Haurwitz, B., Spilhaus, A. F., Willett, H. C., Houghton, H. G., and Malone, T. F., American Meteorological Society, Boston, MA, 207–220,
535 https://doi.org/10.1007/978-1-940033-70-9_18, 1951.
- Niedzielski, T., Szymanowski, M., Miziński, B., Spallek, W., Witek-Kasprzak, M., Ślopek, J., Kasprzak, M., Błaś, M., Sobik, M., Jancewicz, K., Borowicz, D., Remisz, J., Modzel, P., Męcina, K., and Leszczyński, L.: Estimating snow water equivalent using unmanned aerial vehicles for determining snow-melt runoff, *Journal of Hydrology*, 578, 124046, <https://doi.org/10.1016/j.jhydrol.2019.124046>, 2019.
- 540 Pulliainen, J., Luojus, K., Derksen, C., Mudryk, L., Lemmetyinen, J., Salminen, M., Ikonen, J., Takala, M., Cohen, J., Smolander, T., and Norberg, J.: Patterns and trends of Northern Hemisphere snow mass from 1980 to 2018, *Nature*, 581, 294–298, <https://doi.org/10.1038/s41586-020-2258-0>, 2020.
- Pulliainen, J. T., Grandell, J., and Hallikainen, M. T.: HUT snow emission model and its applicability to snow water equivalent retrieval, *IEEE Transactions on Geoscience and Remote Sensing*, 37, 1378–1390, <https://doi.org/10.1109/36.763302>, 1999.



- 545 Raleigh, M. S. and Small, E. E.: Snowpack density modeling is the primary source of uncertainty when mapping basin-wide SWE with lidar, *Geophysical Research Letters*, 44, 3700–3709, <https://doi.org/10.1002/2016GL071999>, 2017.
- Rodriguez, J. D., Perez, A., and Lozano, J. A.: Sensitivity Analysis of k-Fold Cross Validation in Prediction Error Estimation, *IEEE Transactions on Pattern Analysis and Machine Intelligence*, 32, 569–575, <https://doi.org/10.1109/TPAMI.2009.187>, 2010.
- 550 Roebber, P. J., Bruening, S. L., and Jr, J. V. C.: Improving Snowfall Forecasting by Diagnosing Snow Density, *Weather and Forecasting*, 18, 24, [https://doi.org/10.1175/1520-0434\(2003\)018<0264:ISFBDS>2.0.CO;2](https://doi.org/10.1175/1520-0434(2003)018<0264:ISFBDS>2.0.CO;2), 2003.
- Schweizer, J., Bruce Jamieson, J., and Schneebeli, M.: Snow avalanche formation, *Reviews of Geophysics*, 41, 1016, <https://doi.org/10.1029/2002RG000123>, 2003.
- Specht, D. F.: A general regression neural network, 2, 568–576, <https://doi.org/10.1109/72.97934>, 1991.
- 555 Sturm, M., Taras, B., Liston, G. E., Derksen, C., Jonas, T., and Lea, J.: Estimating Snow Water Equivalent Using Snow Depth Data and Climate Classes, *Journal of Hydrometeorology*, 11, 1380–1394, <https://doi.org/10.1175/2010JHM1202.1>, 2010.
- Surendar, M., Bhattacharya, A., Singh, G., and Venkataraman, G.: Estimation of snow density using full-polarimetric Synthetic Aperture Radar (SAR) data, *Physics and Chemistry of the Earth, Parts A/B/C*, 83–84, 156–165, <https://doi.org/10.1016/j.pce.2015.07.001>, 2015.
- 560 Valt, M., Guyennon, N., Salerno, F., Petrangeli, A. B., Salvatori, R., Cianfarra, P., and Romano, E.: Predicting new snow density in the Italian Alps: A variability analysis based on 10years of measurements, *Hydrological Processes*, 32, 3174–3187, <https://doi.org/10.1002/hyp.13249>, 2018.
- Varade, D., Manickam, S., Dikshit, O., Singh, G., and Snehmani: Modelling of early winter snow density using fully polarimetric C-band SAR data in the Indian Himalayas, *Remote Sensing of Environment*, 240, 111699, <https://doi.org/10.1016/j.rse.2020.111699>, 2020.
- 565 Wetlaufer, K., Hendrikx, J., and Marshall, L.: Spatial Heterogeneity of Snow Density and Its Influence on Snow Water Equivalence Estimates in a Large Mountainous Basin, *Hydrology*, 3, 3, <https://doi.org/10.3390/hydrology3010003>, 2016.
- Xin, J., Gong, C., Liu, Z., Cong, Z., Gao, W., Song, T., Pan, Y., Sun, Y., Ji, D., Wang, L., Tang, G., and Wang, Y.: The observation-based relationships between PM_{2.5} and AOD over China, *Journal of Geophysical Research: Atmospheres*, 121, 10,701–10,716, <https://doi.org/10.1002/2015JD024655>, 2016.
- 570 Xiao P., Hu R., Zhang Z., Qin S., and Li Z.: Daily snow albedo products from 2000 to 2020 in China, National Cryosphere Desert Data Center (<http://www.ncdc.ac.cn>) [dataset], <https://doi.org/10.12072/ncdc.I-SNOW.db0004.2020>, 2020.
- Yang, J., Jiang, L., Wu, S., Wang, G., Wang, J., and Liu, X.: Development of a Snow Depth Estimation Algorithm over China for the FY-3D/MWRI, *Remote Sensing*, 11, 977, <https://doi.org/10.3390/rs11080977>, 2019.
- 575 Yang, J. W., Jiang, L. M., Lemmetyinen, J., Luoju, K., Takala, M., Wu, S. L., and Pan, J. M.: Validation of remotely sensed estimates of snow water equivalent using multiple reference datasets from the middle and high latitudes of China, *Journal of Hydrology*, 590, 125499, <https://doi.org/10.1016/j.jhydrol.2020.125499>, 2020.



- Zaremehrdary, M., Razavi, S., and Faramarzi, M.: Assessment of the cascade of uncertainty in future snow depth projections across watersheds of mountainous, foothill, and plain areas in northern latitudes, *Journal of Hydrology*, 598, 125735, 580 <https://doi.org/10.1016/j.jhydrol.2020.125735>, 2021.
- Zhong, X., Zhang, T., and Wang, K.: Snow density climatology across the former USSR, *The Cryosphere*, 8, 785–799, <https://doi.org/10.5194/tc-8-785-2014>, 2014.
- Zhong X., Zhang T., Su H., Xiao X., Wang S., Hu Y., Wang H., Zheng L., Zhang W., Xu M., and Wang J.: Impacts of landscape and climatic factors on snow cover in the Altai Mountains, China, *Advances in Climate Change Research*, 12, 95–585 107, <https://doi.org/10.1016/j.accre.2021.01.005>, 2021a.
- Zhong, X., Zhang, T., Kang, S., and Wang, J.: Spatiotemporal variability of snow cover timing and duration over the Eurasian continent during 1966–2012, *Science of The Total Environment*, 750, 141670, <https://doi.org/10.1016/j.scitotenv.2020.141670>, 2021b.